

Fast Detection of Overlapping Communities via Online Tensor Methods

Furong Huang, U. N. Niranjan, Mohammad Umar Hakeem,
Animashree Anandkumar*

Abstract

We present a fast tensor-based approach for detecting hidden overlapping communities under the Mixed Membership Stochastic Blockmodel (MMSB). We present two implementations, viz., a GPU-based implementation which exploits the parallelism of SIMD architectures and a CPU-based implementation for larger datasets, wherein the GPU memory does not suffice. Our GPU-based implementation involves a careful optimization of storage, data transfer and matrix computations. Our CPU-based implementation involves sparse linear algebraic operations which exploit the data sparsity. We use stochastic gradient descent for multilinear spectral optimization and this allows for flexibility in the tradeoff between node sub-sampling and accuracy of the results. We validate our results on datasets from Facebook, Yelp and DBLP where ground truth is available, using notions of p -values and false discovery rates, and obtain high accuracy for membership recovery. We compare our results, both in terms of execution time and accuracy, to the state-of-the-art algorithms such as the variational method, and report many orders of magnitude gain in the execution time. For instance, for the DBLP dataset with about a million nodes and 16 million edges, the execution time is about two minutes.

Keywords: Community detection, Mixed Membership Stochastic Blockmodel, tensor method, stochastic gradient descent, parallel implementation, sparsity, p -value, large datasets.

1 Introduction

Studying community formation is an important problem in social networks, and has received widespread attention in sociology, starting from the seminal work of Moreno [22]. A community generally refers to a group of individuals with shared interests or beliefs such as music, sports and religion, or relationships such as friends and co-workers. In a social network, we can typically observe and measure the interactions among the actors, but not the communities they belong to. A challenging problem is then to estimate the communities of the actors using only their observed interactions. In general, actors can participate in multiple communities, and detecting overlapping communities is even more challenging. Our goal is to design algorithms which can accurately detect overlapping communities, and yet be easily parallelizable so as to achieve speed and scalability on large graphs with millions of nodes. Moreover, we learn a probabilistic community model which allows us to carry out prediction tasks such as link classification.

Although there are many previous works on fast community detection methods, such as label propagation [28], local searches based on random walk [25] and so on, these are non-probabilistic and heuristic approaches. On the other hand existing probabilistic approaches, such as the variational approach, are very slow and not easily parallelizable. In this paper, we achieve both the objectives, namely, learning a probabilistic mixed membership model and learning in a fast, scalable and parallel manner. This is carried out via a moment based approach which, in our setting, reduces to finding a low-rank tensor decomposition that is carried out efficiently.

*The authors are with Electrical Engineering and Computer Science Dept., University of California, Irvine, USA 92697. Email: furongh@uci.edu, un.niranjan@uci.edu, mhakeem@uci.edu, a.anandkumar@uci.edu

Summary of Contributions: In this work, we present a fast approach for detecting overlapping communities under the Mixed Membership Stochastic Blockmodel (MMSB) [1]. It is based on estimating tensors implicitly from subgraph counts such as 3-stars in the observed network using performing linear algebraic operations such as SVD followed by an iterative stochastic gradient descent method for tensor decomposition using implicit trilinear operations. We present two implementations, viz., a GPU-based implementation which exploits the parallelism of SIMD architectures and a CPU-based implementation for larger datasets, where the GPU memory does not suffice. The running time of our method is $O(n + k^3)$ using nk cores in the parallel computation model [16], where n is the number of nodes and k is the number of communities. Since $k \ll n$, we have a linear running time in the number of nodes, which makes it scalable in the context of extremely large networks.

We first describe our GPU implementation. Our method is highly parallel and Graphics Processing Units (GPUs) are ideal for the deployment of our method since they contain thousands of cores. We carry out a careful GPU-based code optimization and design of data structures for efficient heterogeneous storage on both the CPU and the GPU memories, and minimize CPU-GPU data transfers to obtain significant speedups. A naive implementation of the tensor method would result in a huge space requirement since it requires the manipulation of an $O(n) \times O(n) \times O(n)$ tensor, where n is the number of nodes. This also results in poor scaling of the running time due to the communication costs between the CPU and the GPU. Hence, we never explicitly construct the $O(n) \times O(n) \times O(n)$ tensor; we carry out dimensionality reduction in the preprocessing stage and then manipulate a $k \times k \times k$ tensor, where k is the number of communities. We carry out the decomposition of this smaller tensor implicitly, without forming it, using stochastic gradient descent. Moreover, we convert the stochastic gradient update steps to matrix and vector operations, and implement them using the GPU *device interface*, so as to reduce the GPU-CPU data transfer overhead, and obtain a bigger speed-up. Thus, we present an extremely fast community detection method on GPUs.

We now describe our CPU implementation. This was carried out to overcome the memory limitations of the GPU for extremely large datasets consisting of millions of nodes. We manipulate the data in the sparse format, consisting of sparse multiplications and sparse Lanczos SVD. Furthermore, we implement randomized methods for dimensionality reduction [10]. We obtain tremendous gains in terms of both the running time and the memory required to run on datasets with millions of nodes. We observe that while our GPU implementation is efficient for denser graphs, with larger number of communities, such as Facebook, our CPU implementation is efficient for sparse graphs, with large number of nodes, such as Yelp and DBLP which would not fit in the GPU memory wholly.

We recover hidden communities in several real and synthetic datasets with high accuracy. When ground-truth communities are available, we propose a new error score based on the hypothesis testing methodology involving p -values and false discovery rates [29] to validate our results. Although these notions are standard in statistics, especially in bio-statistics, their use in social network analysis has been limited. The use of p -values eliminates the need to carefully tune the number of communities output by our algorithm, and hence, we obtain a flexible trade-off between the fraction of communities recovered and their estimation accuracy. We also provide arguments to show that the Normalized Mutual Information (NMI) and other scores, previously used for evaluating the recovery of overlapping community, can underestimate the errors and, in fact, the overlapping version of NMI does not reduce to the information-theoretic non-overlapping version of NMI, and is thus incorrect.

We find that our method has very good accuracy on a range of datasets: Facebook, Yelp and DBLP. For the Facebook friendship dataset, consisting of around 0.7 million edges, 20000 nodes and 360 communities, the average error in estimating the community memberships is below 5% and the running time of our algorithm is 35 seconds. For the dataset consisting of Yelp reviews, consisting of around 0.6 million edges, 40000 nodes and 159 communities, the error is below 10% and the running time of our algorithm is 10 seconds. On a much larger DBLP collaborative dataset, consisting of 16 million edges, one million nodes and 250 communities, the error is about 10% and the method runs in about two minutes, excluding the 80 minutes taken to read the edge data from files stored on the hard disk. Note that once we read all the edge information and load them on to the memory, our method computes the communities for the entire set comprising of a million nodes simultaneously in about two minutes. This differs from other community

detection methods, such as methods based on random walk, which do not necessarily read the entire edge information in the beginning of. These methods are local in that they start with a single seed node and then traverse the graph [31]. We note that alternative local implementations of our tensor-based method are possible, and we defer it to future work.

Compared to the state-of-the-art method for learning MMSB models using the stochastic variational inference algorithm of [15], we obtain several orders of magnitude speed-up in the running time on multiple real datasets. This is because our method consists of efficient matrix operations which are *embarrassingly parallel*. Matrix operations are also carried out in the sparse format which is efficient especially for social network settings involving large sparse graphs. Moreover, our code is flexible to run on a range of graphs such as directed, undirected and bipartite graphs, while the code of [15] is designed for homophilic networks, and cannot handle bipartite graphs, needed for us to recover communities in a recommendation setting such as the Yelp dataset.

Although there have been fast implementations for community detection before [28, 19], these methods are not statistical and do not yield descriptive statistics such as bridging nodes [23], and cannot perform predictive tasks such as link classification which are the main strengths of the MMSB model. With the implementation of our tensor-based approach, we record huge speed-ups compared to existing approaches for learning the MMSB model.

Related work: This paper builds on the recent work of Anandkumar et al [2] which establishes the correctness of tensor-based approaches for learning MMSB [1] models. While, the earlier work [2] provided a theoretical analysis of the method, the current paper considers a careful implementation of the method. Moreover, there are a number of algorithmic improvements in this paper. For instance, while [2] considers tensor power iterations, based on batch data and deflations performed serially, here, we adopt a novel approach based on stochastic gradient descent for tensor decomposition, which provides flexibility to trade-off node sub-sampling with accuracy. Moreover, we use randomized methods for dimensionality reduction in the preprocessing stage of our method which enables us to scale our method to graphs with millions of nodes.

There are other known methods for learning the stochastic block model based on techniques such as spectral clustering [21] and convex optimization [9]. However, these methods are not applicable for learning overlapping communities.

We note that learning the mixed membership model can be reduced to a matrix factorization problem [32]. While collaborative filtering techniques focus on matrix factorization and the prediction accuracy of recommendations on an unseen test set, we recover the underlying latent communities, which helps with the interpretability of the network structure. Since our goal is to recover latent communities, we compare the results against the ground truth in order to evaluate our results. Once the communities are discovered, it is straightforward to use our method for the purpose of link prediction.

To the best of our knowledge, while stochastic methods for matrix decomposition have been considered earlier [24, 4], this is the first work incorporating stochastic optimization for tensor decomposition, and paves the way for further investigation on many theoretical and practical issues. We also note that we never explicitly form or store the subgraph count tensor, of size $O(n^3)$ where n is the number of nodes, in our implementation, but directly manipulate the neighborhood vectors to obtain tensor decompositions through stochastic updates. This is a crucial departure from other works on tensor decompositions on GPUs [6, 26], where the tensor needs to be stored and manipulated directly.

2 Mixed Membership Model

Our approach posits a probabilistic model, where the users may belong to multiple communities [1]. The intuition behind the model is that the interactions among the actors in a social network is dependent on their memberships in various communities. We note that there exists a guaranteed algorithm [2] for learning the hidden communities in a social network. In our modeling, the actors in a network correspond to nodes in a graph and the interactions among them correspond to edges in the graph.

Let n denote the number of nodes, k the number of communities and $G \in \mathbb{R}^{n \times n}$ the adjacency matrix of the graph. In the mixed membership community model, the membership vector π_u of node u is contained in a simplex, i.e., $\sum_{i \in [k]} \pi_u(i) = 1, \forall u \in [n]$ where the notation $[n]$ denotes the set $\{1, \dots, n\}$. Membership vectors are sampled from the Dirichlet distribution $\pi_u \stackrel{iid}{\sim} \text{Dir}(\alpha), \forall u \in [n]$ with parameter vector $\alpha \in \mathbb{R}_+^k$. We define the Dirichlet concentration (mixing) parameter $\alpha_0 := \sum_{i \in [k]} \alpha_i$. The Dirichlet distribution allows us to specify the extent of overlap among the communities by controlling for sparsity in community membership vectors. A larger α_0 results in more overlapped (mixed) memberships. A special case of $\alpha_0 = 0$ is the stochastic block model [2]. The *community connectivity matrix* is denoted by $P \in [0, 1]^{k \times k}$ where $P(a, b)$ measures the connectivity between communities a and $b, \forall a, b \in [k]$. We model the adjacency matrix entries as follows:

1. *Bernoulli model*: This models a network with unweighted edges. It is used for Facebook and DBLP datasets in Section 6 in our experiments. $G_{ij} \stackrel{iid}{\sim} \text{Ber}(\pi_i^\top P \pi_j), \forall i, j \in [n]$.
2. *Poisson model [17]*: This models a network with weighted edges. It is used for the Yelp dataset in Section 6 to incorporate the review ratings. $G_{ij} \stackrel{iid}{\sim} \text{Poi}(\pi_i^\top P \pi_j), \forall i, j \in [n]$.

3 Learning using Third Order Moment

Our learning algorithm uses the third order moment to estimate the community membership matrix Π . First, we obtain subgraph counts obtained by partitioning the dataset (Appendix A). Then, we perform tensor decomposition efficiently using *stochastic gradient descent* [18] along with simple bilinear and trilinear transformations involving vectors of length $O(n)$. We note that, in our implementation of the algorithm on the Graphics Processing Unit (GPU), linear algebraic operations are extremely fast. We also implement our algorithm on the CPU using the sparse matrix operations which results in large gains in terms of both the memory and the running time requirements. We now summarize the datasets used in this paper in Table 1.

Statistics	Facebook	Yelp	DBLP sub	DBLP
$ E $	766,800	672,515	5,066,510	16,221,000
$ V $	18,163	10,010+28,588	116,317	1,054,066
GD	0.004649	0.000903	0.000749	0.000029
k	360	159	250	6,003
AB	0.5379	0.4281	0.3779	0.2066
ADCB	47.01	30.75	48.41	6.36

Table 1: Summary of real datasets used in our paper: $|V|$ is the number of nodes in the graph, $|E|$ is the number of edges, GD is the graph density given by $\frac{2|E|}{|V|(|V|-1)}$, k is the number of communities, AB is the average bridgeness and ADCB is the average degree-corrected bridgeness(explained in Section 5).

The overall summary of our approach is as follows:

1. Partition the graph (Appendix A) and estimate the 3-star count tensor (implicitly). The tensor is not formed explicitly as we break down the tensor operations into vector and matrix operations.
2. Pre-process to reduce dimensionality via symmetrization and orthogonalization.
3. Use stochastic gradient descent to estimate spectrum of whitened 3-star count (implicit) tensor.
4. Apply post-processing to obtain the community membership estimates of the nodes in the graph.
5. If ground truth is known, validate the results using various evaluation measures.

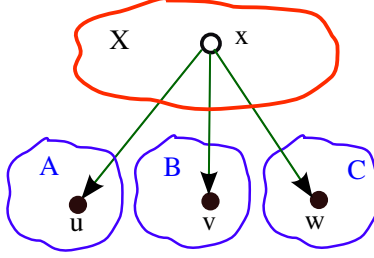


Figure 1: 3-star count tensor from X to three disjoint sets A, B, C .

3.1 Estimation of 3-stars

Our learning approach involves a third order moment estimation using subgraph counts obtained by partitioning the dataset (Appendix A). We note that this tensor is never formed explicitly but manipulated implicitly. For details as to why the $O(n^3)$ tensor is never constructed, but instead, the multilinear transformations are performed on the vectors corresponding to the modes of the tensor, refer Section 3.3. Consider a partition of the nodes into sets X, A, B, C . A 3-star is a star graph with an internal node $x \in X$ and three leaves $\{u, v, w\}$ with $u \in A, v \in B, w \in C$. We refer to the internal node x of the star as its “head”, and denote the structure by $x \rightarrow \{u, v, w\}$ (see Figure 1). We count the number of 3-stars from X to A, B, C and we aim to learn the spectrum of the third order moment (tensor) without actually forming it.

3.2 Dimensionality Reduction

The hidden communities are estimated via the decomposition of the third order moment tensor¹ from the three-view data involving the *whitened* neighbourhood vectors obtained using $G_{x,A}$, $G_{x,B}$ and $G_{x,C}$ drawn from the adjacency matrix G . A unique and tractable tensor decomposition [3] exists for symmetric and orthogonal tensors, leading to a guaranteed recovery of the communities.

1. *Symmetrization*: Using Theorem 3.6 of [3], we symmetrize the third order moment via efficient linear algebraic operations using the second order moments (see Appendix B for details). For this purpose, we use the transformations computed using the *pairs matrix* which are given by

$$\begin{aligned} Z_B &:= \text{Pairs}(A, C) (\text{Pairs}(B, C))^\dagger, \\ Z_C &:= \text{Pairs}(A, B) (\text{Pairs}(C, B))^\dagger. \end{aligned}$$

2. *Orthogonalization*: After symmetrization, we orthogonalize the third moment to reduce the dimension of its modes to k . For this purpose, we compute the whitening matrix W such that $W^\top M_2^{\alpha_0} W = I$ where $M_2^{\alpha_0}$ (for details and notation, refer Appendix B) is given by

$$M_2^{\alpha_0} = \frac{1}{n_X} \sum_{x \in X} Z_C G_{x,C}^\top G_{x,B} Z_B^\top - \frac{\alpha_0}{\alpha_0 + 1} (\mu_{X \rightarrow A} \mu_{X \rightarrow A}^\top - \text{diag}(\mu_{X \rightarrow A} \mu_{X \rightarrow A}^\top)).$$

The whitening matrix, derived in Appendix B, is computed using the second order moments, i.e., 2-stars. We then perform multilinear transformations on the data corresponding to the partitions A, B and C using the whitening matrix. The whitened data is thus $g_A^t := \langle G_{x,A}^\top, W \rangle$, $g_B^t := \langle Z_B G_{x,B}^\top, W \rangle$, and $g_C^t := \langle Z_C G_{x,C}^\top, W \rangle$, where $x \in X$ and t denotes the index of the online data. Since $k \ll n$, the dimensionality reduction is crucial for our speedup.

¹Although this is a tensor, we never explicitly compute the Kronecker product since we only need inner products involving the vectors corresponding to the modes of the third order tensor. This leads to efficient “tensor” computations.

3.3 Stochastic Tensor Gradient Descent

In [2] and [3], the power method with deflation is used for tensor decomposition where the eigenvectors are recovered by iterating over multiple loops in a serial manner. Furthermore, batch data is used in their iterative power method which makes that algorithm slower than its stochastic counterpart. In addition to implementing a stochastic spectral optimization algorithm, we achieve further speed-up by efficiently parallelizing the stochastic updates (Appendix C.1).

Let $\mathbf{v} = [v_1|v_2|\dots|v_k]$ be the true eigenvectors. Denote the cardinality of the set X as n_x , i.e., $n_x := |X|$. Now that we have the whitened tensor, we propose the *Stochastic Tensor Gradient Descent* (STGD) algorithm for tensor decomposition. Consider the tensor $\mathcal{T} \in \mathbb{R}^{k \times k \times k}$ using whitened samples from X , i.e.,

$$\mathcal{T} = \sum_{t \in X} \mathcal{T}^t = \sum_{t \in X} g_A^t \otimes g_B^t \otimes g_C^t,$$

where $x \in X$ and t denotes the index of the online data.

Our goal is to find a symmetric CP decomposition of the whitened tensor. Our optimization problem is given by

$$\arg \min_{\mathbf{v}} \left\{ \left\| 2\theta \sum_{i \in [k]} \otimes^3 v_i - \sum_{t \in X} \mathcal{T}^t \right\|_F^2 \right\},$$

where v_i are the unknown components to be estimated, and $\theta > 0$ is some fixed parameter. The role of θ will be clarified subsequently. Since $\|\sum_{t \in X} \mathcal{T}^t\|_F^2$ is a constant, the above minimization is the same as minimizing a loss function $L(\mathbf{v}) := \frac{1}{n_x} \sum_t L^t(\mathbf{v})$, where $L^t(\mathbf{v})$ is the loss function evaluated at node $t \in X$, and is given by

$$L^t(\mathbf{v}) := \theta \left\| \sum_{i \in [k]} \otimes^3 v_i \right\|_F^2 - \left\langle \sum_{i \in [k]} \otimes^3 v_i, \mathcal{T}^t \right\rangle \quad (1)$$

The loss function has two terms, viz., the term $\|\sum_{i \in [k]} \otimes^3 v_i\|_F^2$, which can be interpreted as the orthogonality cost, which we need to minimize, and the second term $\langle \sum_{i \in [k]} \otimes^3 v_i, \mathcal{T}^t \rangle$, which can be viewed as the correlation reward to be maximized. The parameter θ provides additional flexibility for tuning between the two terms.

Let $\Phi^t := [\phi_1^t | \phi_2^t | \dots | \phi_k^t]$ denote the estimation of the eigenvectors using the whitened data point t , where $\phi_i^t \in \mathbb{R}^k$, $i \in [k]$. Taking the derivative of the loss function leads us to the iterative update equation for the stochastic gradient descent which is

$$\phi_i^{t+1} \leftarrow \phi_i^t - \beta^t \frac{\partial L^t}{\partial v_i} \Big|_{\phi_i^t}, \quad \forall i \in [k]$$

where β^t is the learning rate.

We update eigenvectors through

$$\phi_i^{t+1} \leftarrow \phi_i^t - 3\theta\beta^t \sum_{j=1}^k \left[\langle \phi_j^t, \phi_i^t \rangle^2 \phi_j^t \right] + \beta^t \langle \phi_i^t, g_A^t \rangle \langle \phi_i^t, g_B^t \rangle g_C^t + \beta^t \langle \phi_i^t, g_B^t \rangle \langle \phi_i^t, g_C^t \rangle g_A^t + \beta^t \langle \phi_i^t, g_C^t \rangle \langle \phi_i^t, g_A^t \rangle g_B^t.$$

In the above expression, all our tensor operations are in terms of efficient sample vector inner products, and no tensor is explicitly formed. We choose $\theta = 1$ in our experiments to ensure that there is sufficient penalty for non-orthogonality, which prevents us from obtaining degenerate solutions.

After learning the decomposition of the third order moment, we perform post-processing to estimate $\hat{\Pi}$. Refer to Appendix C.2 for details.

4 Implementation Details

Computational complexity: We partition the execution of our algorithm into three main modules namely, pre-processing, STGD and post-processing, whose various matrix operation counts are listed above

Module	BLAS I	BLAS II	BLAS III	SVD	QR
Pre	0	8	19	3	0
STGD	0	Nk	$7N$	0	2
Post	0	0	7	0	0

Table 2: Linear algebraic operation counts: N denotes the number of iterations for STGD and k , the number of communities. For details on how we manipulate matrices for STGD, see Appendix C.1.

Module	Pre	STGD	Post
Time	$O(n + k^3)$	$O(k)$	$O(n)$
Space	$O(nk)$	$O(k^2)$	$O(nk)$

Table 3: The time and space complexity of our algorithm. Note that $k \ll n$ and the STGD column denotes the per-iteration complexity.

in Table 2. The theoretical asymptotic complexity (Table 3) of our method is best addressed by considering the parallel model of computation [16]. This is justified considering that we implement our method on GPUs and matrix products are embarrassingly parallel.

Memory Issues: The main bottleneck for our implementation is device storage, since GPU memory is highly limited and not expandable. However, recall that the STGD step is dependent only on k , and hence can fit in the GPU memory. So, only the pre-processing and the post-processing modules are essentially the limiting ones, especially the large SVD computations (refer Table 2). We emphasize that we implement our algorithm on a single machine whose specifications are given in Table 7 in Appendix E. In order to support larger datasets such as the DBLP dataset which exceed the GPU memory capacity, we extend our implementation with out-of-GPU-core matrix operations and the Nystrom method [13] for the whitening matrix computation and the pseudoinverse computation in the pre-processing module. This can be solved via distributed QR method [11], which involves the (dense) SVD of a $k \times k$ ($k \ll n$) matrix leading to $O(k^3)$ in Table 3 followed by multiplication to find Q , which takes $O(n)$ time.

Alternative sparse implementation: To resolve the memory issue of GPU and incorporate the computational challenge of the DBLP dataset with a million nodes, we use sparse manipulations, since the edge density is extremely small. GPU although has SIMD architecture which makes parallelization efficient, it lacks advanced libraries with sparse SVD operations and out-of-GPU-core implementations. We therefore implement sparse format on CPU for sparse datasets. We employ random projection for efficient dimensionality reduction [10] and employ sparse format multiplication available in the Eigen toolkit and SVD [8] which uses the Lanczos algorithm on the CPU. Theoretically, the Lanczos algorithm [14] on a $n \times n$ matrix takes around $(2d + 8)n$ flops for a single step where d is the average number of non-zero entries per row.

4.1 Stochastic updates

STGD can potentially be the most computationally intensive task if carried out naively since the storage and manipulation of a $O(n^3)$ -sized tensor makes the method not scalable. However we overcome this problem since we never form the tensor explicitly. We gain large speed up by optimizing the implementation of STGD. To implement the tensor operations efficiently we convert them into matrix and vector operations so that they are implemented using BLAS routines on GPU. We obtain whitened 3-star vectors from the partitions A , B and C , and manipulate these vectors efficiently to obtain tensor eigenvector updates using the gradient scaled by a suitable learning rate. Moreover, we convert the BLAS II into BLAS III operations by stacking the vectors to form matrices, thus avoiding loops. Refer to Appendix C.1.

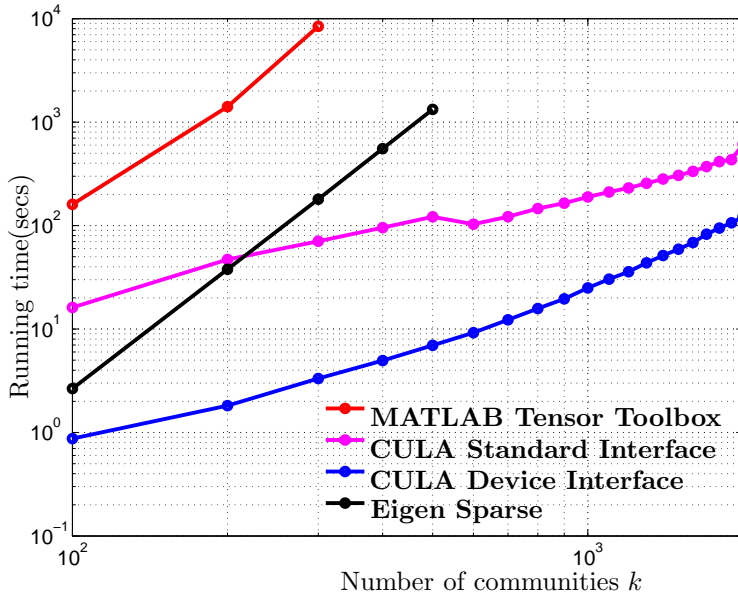


Figure 2: Comparison of the running time for STGD under different k for 100 iterations.

In STGD, note that the storage needed for the iterative part does not depend on the number of nodes in the dataset, rather, it depends on the parameter k , i.e., the number of communities to be estimated, since whitening performed before STGD leads to dimensionality reduction. This makes it suitable for storing the required buffers in the GPU memory, and using the CULA device interface for the BLAS operations.

We compare the running time of the CULA device code with the MATLAB code (using the tensor toolbox [5]), CULA standard code and Eigen sparse code in Figure 2. As expected, the GPU implementations of matrix operations are much faster and scale much better than the CPU implementations. Among the CPU codes, we notice that sparsity and optimization offered by the Eigen toolkit gives us huge gains. We obtain orders of magnitude of speed up for the GPU device code as we place the buffers in the GPU memory and transfer minimal amount of data involving the whitened vectors only once at the beginning of each iteration. The running time for the CULA standard code is more than the device code because of the CPU-GPU data transfer overhead. For the same reason, the sparse CPU implementation, by avoiding the data transfer overhead, performs better than the GPU standard code for very small number of communities. For details on the preprocessing and postprocessing steps, refer to Appendix E.

5 Validation methods

5.1 p -value testing:

We recover the estimated community membership matrix $\hat{\Pi} \in \mathbb{R}^{\hat{k} \times n}$, where \hat{k} is the number of communities specified to our method. Recall that the true community membership matrix is Π , and we consider datasets where ground truth is available. Let i -th row of $\hat{\Pi}$ be denoted by $\hat{\Pi}_i$. Our community detection method is unsupervised, which inevitably results in row permutations between Π and $\hat{\Pi}$ and \hat{k} may not be the same as k . To validate the results, we need to find a good match between the rows of $\hat{\Pi}$ and Π . We use the notion of p -values to test for statistically significant dependencies among a set of random variables. The p -value denotes the probability of not rejecting the null hypothesis that the random variables under

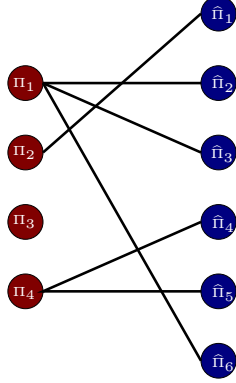


Figure 3: Bipartite graph $G_{\{P_{\text{val}}\}}$ induced by p -value testing. Edges represent statistically significant relationships between ground truth and estimated communities.

consideration are independent and we use the Student's² t -test statistic [12] to compute the p -value. We use multiple hypothesis testing for different pairs of estimated and ground-truth communities $\hat{\Pi}_i, \Pi_j$ and adjust the p -values to ensure a small enough false discovery rate (FDR) [29].

The test statistic used for the p -value testing of the estimated communities is

$$T_{ij} := \frac{\rho(\hat{\Pi}_i, \Pi_j) \sqrt{n-2}}{\sqrt{1 - \rho(\hat{\Pi}_i, \Pi_j)^2}}.$$

The right p -value is obtained via the probability of obtaining a value (say t_{ij}) greater than the test statistic T_{ij} , and it is defined as

$$P_{\text{val}}(\Pi_i, \hat{\Pi}_j) := 1 - \mathbb{P}(t_{ij} > T_{ij}).$$

Note that T_{ij} has Student's t -distribution with degree of freedom $n-2$ (i.e. $T_{ij} \sim t_{n-2}$). Thus, we obtain the right p -value³.

In this way, we compute the \mathbf{P}_{val} matrix as

$$\mathbf{P}_{\text{val}}(i, j) := P_{\text{val}}[\hat{\Pi}_i, \Pi_j], \forall i \in [k] \text{ and } j \in [\hat{k}].$$

5.2 Evaluation metrics

Recovery ratio: Validating the results requires a matching the true membership Π with estimated membership $\hat{\Pi}$. Let $P_{\text{val}}(\Pi_i, \hat{\Pi}_j)$ denotes the right p -value under the null hypothesis that Π_i and $\hat{\Pi}_j$ are statistically independent. We use the p -value test to find out pairs $\Pi_i, \hat{\Pi}_j$ which pass a specified p -value threshold, and we denote such pairs using a bipartite graph $G_{\{P_{\text{val}}\}}$. Thus, $G_{\{P_{\text{val}}\}}$ is defined as

$$G_{\{P_{\text{val}}\}} := \left(\left\{ V_{\{P_{\text{val}}\}}^{(1)}, V_{\{P_{\text{val}}\}}^{(2)} \right\}, E_{\{P_{\text{val}}\}} \right),$$

where the nodes in the two node sets are

$$\begin{aligned} V_{\{P_{\text{val}}\}}^{(1)} &= \{\Pi_1, \dots, \Pi_k\}, \\ V_{\{P_{\text{val}}\}}^{(2)} &= \{\hat{\Pi}_1, \dots, \hat{\Pi}_{\hat{k}}\} \end{aligned}$$

²Note that Student's t -test is robust to the presence of unequal variances when the sample sizes of the two are equal which is true in our setting.

³The right p -value accounts for the fact that when two communities are anti-correlated they are not paired up. Hence note that in the special case of block model in which the estimated communities are just permuted version of the ground truth communities, the pairing results in a perfect matching accurately.

and the edges of $G_{\{P_{\text{val}}\}}$ satisfy

$$(i, j) \in E_{\{P_{\text{val}}\}} \text{ s.t. } P_{\text{val}} \left[\widehat{\Pi}_i, \Pi_j \right] \leq 0.01.$$

A simple example is shown in Figure 3, in which Π_2 has statistically significant dependence with $\widehat{\Pi}_1$, i.e., the probability of not rejecting the null hypothesis is small (recall that null hypothesis is that they are independent). If no estimated membership vector has a significant overlap with Π_3 , then Π_3 is not recovered. There can also be multiple pairings such as for Π_1 and $\{\widehat{\Pi}_2, \widehat{\Pi}_3, \widehat{\Pi}_6\}$. The p -value test between Π_1 and $\{\widehat{\Pi}_2, \widehat{\Pi}_3, \widehat{\Pi}_6\}$ indicates that probability of not rejecting the null hypothesis is small, i.e., they are independent. We use 0.01 as the threshold. The same holds for Π_2 and $\{\widehat{\Pi}_1\}$ and for Π_4 and $\{\widehat{\Pi}_4, \widehat{\Pi}_5\}$. There can be a perfect one to one matching like for Π_2 and $\widehat{\Pi}_1$ as well as a multiple matching such as for Π_1 and $\{\widehat{\Pi}_2, \widehat{\Pi}_3, \widehat{\Pi}_6\}$.

The *recovery ratio* is defined as

$$\mathcal{R} := \frac{1}{k} \sum_{(i,j) \in E_{\{P_{\text{val}}\}}} 1$$

for all $i \in [k]$ and $j \in [\widehat{k}]$, where P_{val} denotes the p -value. The perfect case is that all the memberships have at least one significant overlapping estimated membership, giving a recovery ratio of 100%.

Error function: For performance analysis of our learning algorithm we define the average error function as

$$\mathcal{E} := \frac{1}{k} \sum_{(i,j) \in E_{\{P_{\text{val}}\}}} \left\{ \frac{1}{n} \sum_{x \in |X|} \left| \widehat{\Pi}_i(x) - \Pi_j(x) \right| \right\}, \forall i \in [k], j \in [\widehat{k}],$$

where P_{val} denotes the p -value.

The error function incorporates two aspects, namely the l_1 norm error between each estimated community and the corresponding paired ground truth community, and the error induced by false pairings between the estimated and ground-truth communities through p -value testing. For the former l_1 norm error, we normalize with n which is reasonable and results in the range of the error in $[0, 1]$. For the latter, we define the average error function as the summation of all paired memberships errors divided by the true number of communities k . In this way we penalize falsely discovered pairings by summing them up. Our error function can be greater than 1 if there are too many falsely discovered pairings through p -value testing (which can be as large as $k \times \widehat{k}$).

Bridgeness: Bridgeness in overlapping communities is an interesting measure to evaluate. A bridge is defined as a vertex that crosses structural holes between discrete groups of people and bridgeness analyzes the extent to which a given vertex is shared among different communities [23]. Formally, the bridgeness of a vertex i is defined as

$$b_i := 1 - \sqrt{\frac{\widehat{k}}{\widehat{k} - 1} \sum_{j=1}^{\widehat{k}} \left(\widehat{\Pi}_i(j) - \frac{1}{\widehat{k}} \right)^2}. \quad (2)$$

Note that centrality measures should be used in conjunction with bridge score to distinguish outliers from genuine bridge nodes [23]. The *degree-corrected bridgeness* is used to evaluate our results and is defined as

$$\mathcal{B}_i := D_i b_i, \quad (3)$$

where D_i is degree of node i .

5.3 Comparison of error scores

Normalized Mutual Information (NMI) score [20] is another popular score which is defined differently for overlapping and non-overlapping community models. For non-overlapping block model, ground truth membership for node i is a discrete k -state categorical variable $\Pi_{\text{block}} \in [k]$ and the estimated membership is a discrete \hat{k} -state categorical variable $\hat{\Pi}_{\text{block}} \in [\hat{k}]$. The empirical distribution of ground truth membership categorical variable Π_{block} is easy to obtain. Similarly is the empirical distribution of the estimated membership categorical variable $\hat{\Pi}_{\text{block}}$. NMI for block model is defined as

$$N_{\text{block}}(\hat{\Pi}_{\text{block}} : \Pi_{\text{block}}) := \frac{H(\Pi_{\text{block}}) + H(\hat{\Pi}_{\text{block}}) - H(\Pi_{\text{block}}, \hat{\Pi}_{\text{block}})}{\left(H(\Pi_{\text{block}}) + H(\hat{\Pi}_{\text{block}})\right) / 2}.$$

The NMI for overlapping communities is a binary vector instead of a categorical variable [20]. The ground truth membership for node i is a binary vector of length k , $\mathbf{\Pi}_{\text{mix}}$, while the estimated membership for node i is a binary vector of length \hat{k} , $\hat{\mathbf{\Pi}}_{\text{mix}}$. This notion coincides with one column of our membership matrices $\mathbf{\Pi} \in \mathbb{R}^{k \times n}$ and $\hat{\mathbf{\Pi}} \in \mathbb{R}^{\hat{k} \times n}$ except that our membership matrices are stochastic. In other words, we consider all the nonzero entries of $\mathbf{\Pi}$ as 1's, then each column of our $\mathbf{\Pi}$ is a sample for $\mathbf{\Pi}_{\text{mix}}$. The m -th entry of this binary vector is the realization of a random variable $\Pi_{\text{mix}_m} = (\mathbf{\Pi}_{\text{mix}})_m$, whose probability distribution is

$$P(\Pi_{\text{mix}_m} = 1) = \frac{n_m}{n}, \quad P(\Pi_{\text{mix}_m} = 0) = 1 - \frac{n_m}{n},$$

where n_m is the number of nodes in community m . The same holds for $\hat{\Pi}_{\text{mix}_m}$. The normalized conditional entropy between $\mathbf{\Pi}_{\text{mix}}$ and $\hat{\mathbf{\Pi}}_{\text{mix}}$ is defined as

$$H(\hat{\mathbf{\Pi}}_{\text{mix}} | \mathbf{\Pi}_{\text{mix}})_{\text{norm}} := \frac{1}{k} \sum_{j \in [k]} \min_{i \in [\hat{k}]} \frac{H(\hat{\Pi}_{\text{mix}_i} | \Pi_{\text{mix}_j})}{H(\Pi_{\text{mix}_j})} \quad (4)$$

where Π_{mix_j} denotes the j^{th} entry of $\mathbf{\Pi}_{\text{mix}}$ and similarly for $\hat{\Pi}_{\text{mix}_i}$. The NMI for overlapping community is

$$N_{\text{mix}}(\hat{\mathbf{\Pi}}_{\text{mix}} : \mathbf{\Pi}_{\text{mix}}) := 1 - \frac{1}{2} \left[H(\mathbf{\Pi}_{\text{mix}} | \hat{\mathbf{\Pi}}_{\text{mix}})_{\text{norm}} + H(\hat{\mathbf{\Pi}}_{\text{mix}} | \mathbf{\Pi}_{\text{mix}})_{\text{norm}} \right].$$

There are two aspects in evaluating the error. The first aspect is the l_1 norm error. According to Equation (4), the error function used in NMI score is $\frac{H(\hat{\Pi}_{\text{mix}_i} | \Pi_{\text{mix}_j})}{H(\Pi_{\text{mix}_j})}$. NMI is not suitable for evaluating recovery of different sized communities. In the special case of a pair of extremely sparse and dense membership vectors, depicted in Figure 4, $H(\Pi_{\text{mix}_j})$ is the same for both the dense and the sparse vectors since they are flipped versions of each other (0s flipped to 1s and vice versa). However, the smaller sized community (i.e. the sparser community vector), shown in red in Figure 4, is significantly more difficult to recover than the larger sized community shown in blue in Figure 4. Thus, NMI is not suitable for evaluating recovery of different sized communities. In contrast, our error function employs a normalized l_1 norm error which penalizes more for larger sized communities than smaller ones.

The second aspect is the error induced by false pairings of estimated and ground-truth communities. NMI score selects only the closest estimated community through normalized conditional entropy minimization and it does not account for statistically significant dependence between an estimated community and multiple ground truth communities and vice-versa, and therefore it underestimates error. However, our error score does not limit to a matching between the estimated and ground truth communities: if an estimated community is found to have statistically significant correlation with multiple ground truth communities (as evaluated by the p -value), we penalize for the error over all such ground truth communities. Thus, our error score is a harsher measure of evaluation than NMI. This notion of ‘‘soft-matching’’ between ground-truth and estimated communities also enables validation of recovery of a combinatorial union of communities instead of single ones.

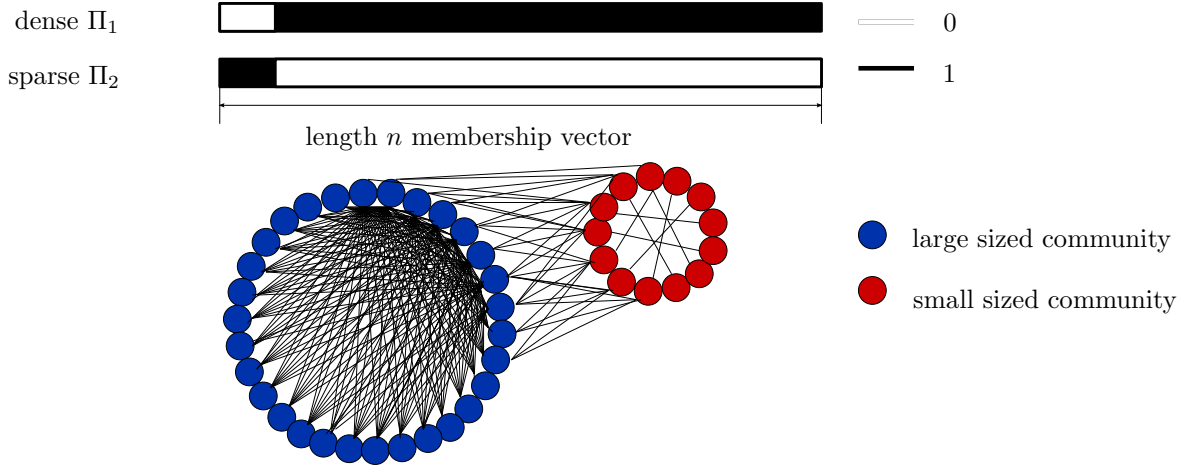


Figure 4: A special case of a pair of extremely dense and sparse communities. Theoretically, the sparse community is more difficult to recover than the dense one. However, the NMI score penalizes both of them equally. Note that for dense Π_1 , $P(\Pi_{\text{mix}_1} = 0) = \frac{\# \text{ of 0s in } \Pi_1}{n}$ which is equal to $P(\Pi_{\text{mix}_2} = 1) = \frac{\# \text{ of 1s in } \Pi_2}{n}$. Similarly, $P(\Pi_{\text{mix}_1} = 1) = \frac{\# \text{ of 1s in } \Pi_1}{n}$ which is equal to $P(\Pi_{\text{mix}_2} = 0) = \frac{\# \text{ of 0s in } \Pi_2}{n}$. Therefore, $H(\Pi_{\text{mix}_1}) = H(\Pi_{\text{mix}_2})$.

A number of other scores such as “separability”, “density”, “cohesiveness” and “clustering coefficient” [31] are non-statistical measures of faithful community recovery. The scores of [31] intrinsically aim to evaluate the level of clustering within a community. However our goal is to measure the accuracy of recovery of the communities and not how well-clustered the communities are.

Banerjee and Langford [7] proposed an objective evaluation criterion for clustering which use classification performance as the evaluation measure. In contrast, we look at how well the method performs in recovering the hidden communities, and we are not evaluating predictive performance. Therefore, this measure is not used in our evaluation.

Finally, we note that cophenetic correlation is another statistical score used for evaluating clustering methods, but note that it is only valid for hierarchical clustering and it is a measure of how faithfully a dendrogram preserves the pairwise distances between the original unmodeled data points [27]. Hence, it is not employed in this paper.

6 Results

We perform synthetic experiments for both stochastic block model and mixed membership model and we obtain highly accurate recovery (Appendix F.1). The specifications of the machine on which we run our code are given in Appendix E. We describe the results on real datasets (Table 1) in detail below and in Table 4.

The results are presented in Table 4. We note that our method, in both dense and sparse implementations, performs very well compared to the state-of-the-art variational method. For the Yelp dataset, we have a bipartite graph where the business nodes are on one side and user nodes on the other and use the review stars as the edge weights. In this bipartite setting, the variational code provided by Gopalan et al [15] does not work on since it is not applicable to non-homophilic models. Our approach does not have this restriction. Note that we use our dense implementation on the GPU to run experiments with large number of communities k as the device implementation is much faster in terms of running time of the STGD step. On the other hand, the sparse implementation on CPU is fast and memory efficient in the case of sparse graphs with a small number of communities while the dense implementation on GPU is faster for denser graphs such as Facebook. Note that data reading time for DBLP is around 4700 seconds, which is not negligible as compared to other datasets (usually within a few seconds). Effectively, our algorithm, excluding the file I/O time, executes within two minutes for $k = 10$ and within ten minutes for $k = 100$.

Data	Method	\widehat{k}	Thre	\mathcal{E}	$\mathcal{R}(\%)$	Time(s)
FB	Ten(sparse)	10	0.10	0.063	13	35
	Ten(sparse)	100	0.08	0.024	62	309
	Ten(sparse)	100	0.05	0.118	95	309
	Ten(dense)	100	0.100	0.012	39	190
	Ten(dense)	100	0.070	0.019	100	190
	Variational	100	–	0.070	100	10,795
	Ten(dense)	500	0.020	0.014	71	468
	Ten(dense)	500	0.015	0.018	100	468
	Variational	500	–	0.031	100	86,808
	YP	Ten(sparse)	10	0.10	0.271	43
Ten(sparse)		100	0.08	0.046	86	287
Ten(dense)		100	0.100	0.023	43	1,127
Ten(dense)		100	0.090	0.061	80	1,127
Ten(dense)		500	0.020	0.064	72	1,706
Ten(dense)		500	0.015	0.336	100	1,706
DB sub		Ten(dense)	100	0.15	0.072	36
	Ten(dense)	100	0.09	0.260	80	7,664
	Variational	100	–	7.453	99	69,156
	Ten(dense)	500	0.10	0.010	19	10,157
	Ten(dense)	500	0.04	0.139	89	10,157
	Variational	500	–	16.38	99	558,723
DB	Ten(sparse)	10	0.30	0.103	73	4716
	Ten(sparse)	100	0.08	0.003	57	5407
	Ten(sparse)	100	0.05	0.105	95	5407

Table 4: Yelp, Facebook and DBLP main quantitative evaluation of "tensor method" vs "variational method" : \widehat{k} is the community number specified to our algorithm, Thre is the threshold for picking significant estimated membership entries. Refer to Table 1 for statistics of the datasets.

Interpretation of the results: The ground truth on business attributes such as location and type of business are available (but not provided to our algorithm) and we provide the distribution in Figure 5 on the left side. There is also a natural trade-off between recovery ratio and average error or between attempting to recover all the business communities and the accuracy of recovery. We can either recover top significant communities with high accuracy or recover more with lower accuracy. We demonstrate the trade-off in Figure 5 on the right side.

We select the top ten categories recovered with the lowest error and report the business with highest weights in $\widehat{\Pi}$. Among the matched communities, we find the business with the highest membership weight (Table 6). We can see that most of the "top" recovered businesses are rated high. Many of the categories in the top ten list are restaurants as they have a large number of reviewers. Our method can recover restaurant category with high accuracy, and the specific restaurant in the category is a popular result (with high number of stars). Also, our method can also recover many of the categories with low review counts accurately like hobby shops, yoga, churches, galleries and religious organizations which are the "niche" categories with a dedicated set of reviewers, who mostly do not review other categories.

The top bridging nodes recovered by our method for the Yelp dataset are given in the Table 5. The bridging nodes have multiple attributes typically, the type of business and its location. In addition, the categories may also be hierarchical: within restaurants, different cuisines such as Italian, American or Pizza are recovered by our method. Moreover, restaurants which also function as bars or lounges are also recovered as top bridging nodes in our method. Thus, our method can recover multiple attributes for the businesses efficiently.

Business	RC	Categories
Four Peaks Brewing Co	735	Restaurants, Bars, American (New), Nightlife, Food, Pubs, Tempe
Pizzeria Bianco	803	Restaurants, Pizza, Phoenix
FEZ	652	Restaurants, Bars, American (New), Nightlife, Mediterranean, Lounges Phoenix
Matt’s Big Breakfast	689	Restaurants, Phoenix, Breakfast& Brunch
Cornish Pasty Company	580	Restaurants, Bars, Nightlife, Pubs, Tempe
Postino Arcadia	575	Restaurants, Italian, Wine Bars, Bars, Nightlife, Phoenix
Cibo	594	Restaurants, Italian, Pizza, Sandwiches, Phoenix
Phoenix Airport	862	Hotels & Travel, Phoenix
Gallo Blanco Cafe	549	Restaurants, Mexican, Phoenix
The Parlor	489	Restaurants, Italian, Pizza, Phoenix

Table 5: Top 10 bridging businesses in Yelp and categories they belong to. “RC” denotes review counts for that particular business.

Category	Business	Star(B)	Star(C)	RC(B)	RC(C)
Latin American	Salvadoreno	4.0	3.94	36	93.8
Gluten Free	P.F. Chang’s	3.5	3.72	55	50.6
Hobby Shops	Make Meaning	4.5	4.13	14	7.6
Mass Media	KJZZ 91.5FM	4.0	3.63	13	5.6
Yoga	Sutra Midtown	4.5	4.55	31	12.6
Churches	St Andrew Church	4.5	4.52	3	4.2
Art Galleries	Sette Lisa	4.5	4.48	4	6.6
Libraries	Cholla Branch	4.0	4.00	5	11.2
Religious	St Andrew Church	4.5	4.40	3	4.2
Wickenburg	Taste of Caribbean	4.0	3.66	60	6.7

Table 6: Most accurately recovered categories and businesses with highest membership weights for the Yelp dataset. “Star(B)” denotes the review stars that the business receive and “Star(C)”, the average review stars that businesses in that category receive. “RC(B)” denotes the review counts for that business and “RC(C)”, the average review counts in that category.

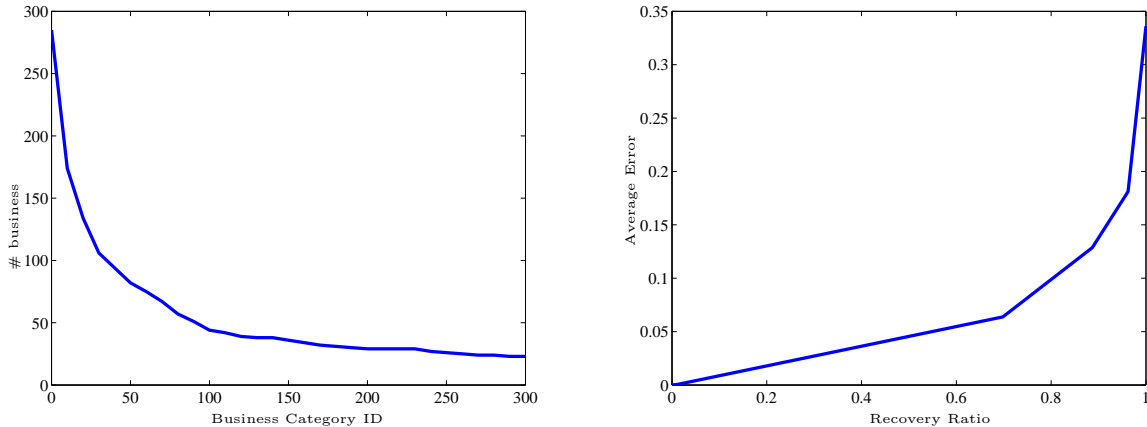


Figure 5: Distribution of business categories (left) and result tradeoff between recovery ratio and error for yelp (right).

For the Facebook dataset, the top ten communities recovered with lowest error consist of certain high schools, second majors and dorms/houses. We observe that high school attributes are easiest to recover and second major and dorm/house are reasonably easy to recover by looking at the friendship relations in Facebook. This is reasonable: college students from the same high school have a high probability of being friends; so do colleges students from the same dorm. For more results, refer to Appendix F.2. For the DBLP subsampled dataset⁴, the performance of our algorithm is summarized in Table 4. Further results are in Appendix F.4. For the full DBLP dataset, we used Eigen Sparse library and scaled up to a million nodes.

Acknowledgement

The first author is supported in part by NSF Career award CCF-1254106 and setup funds at UCI, the second author is supported in part by UCI graduate fellowship and NSF Award CCF-1219234, and the last author is supported in part by Microsoft Faculty Fellowship, NSF Career award CCF-1254106, NSF Award CCF-1219234, and ARO YIP Award W911NF-13-1-0084. The authors acknowledge insightful discussions with Prem Gopalan, David Mimno, David Blei, Qirong Ho, Eric Xing, Carter Butts, Blake Foster, Rui Wang, Sridhar Mahadevan, and the CULA team. Special thanks to Prem Gopalan and David Mimno for providing the variational code and answering all our questions. The authors also thank Daniel Hsu and Sham Kakade for initial discussions regarding the implementation of the tensor method. We also thank Dan Melzer for helping us with the system-related issues.

References

- [1] Edoardo M. Airoldi, David M. Blei, Stephen E. Fienberg, and Eric P. Xing. Mixed membership stochastic blockmodels. *Journal of Machine Learning Research*, 9:1981–2014, June 2008.
- [2] A. Anandkumar, R. Ge, D. Hsu, and S. M. Kakade. A Tensor Spectral Approach to Learning Mixed Membership Community Models. In *Conference on Learning Theory (COLT)*, June 2013.
- [3] A. Anandkumar, R. Ge, D. Hsu, S. M. Kakade, and M. Telgarsky. Tensor decompositions for latent variable models, 2012.

⁴<http://dblp.uni-trier.de/xml/Dblp.xml>

- [4] Raman Arora, Andrew Cotter, Karen Livescu, and Nathan Srebro. Stochastic optimization for pca and pls. In *Communication, Control, and Computing (Allerton), 2012 50th Annual Allerton Conference on*, pages 861–868, 2012.
- [5] Brett W. Bader, Tamara G. Kolda, et al. Matlab tensor toolbox version 2.5. Available online, January 2012.
- [6] Grey Ballard, Tamara Kolda, and Todd Plantenga. Efficiently computing tensor eigenvalues on a gpu. In *Parallel and Distributed Processing Workshops and Phd Forum (IPDPSW), 2011 IEEE International Symposium on*, pages 1340–1348. IEEE, 2011.
- [7] Arindam Banerjee and John Langford. An objective evaluation criterion for clustering. In *Proceedings of the tenth ACM SIGKDD international conference on Knowledge discovery and data mining*, pages 515–520. ACM, 2004.
- [8] Michael Berry, Theresa Do, Gavin O’Brien, Vijay Krishna, and Sowmini Varadhan. Svdlibc version 1.4. Available online, 2002.
- [9] Yudong Chen, Sujay Sanghavi, and Huan Xu. Clustering sparse graphs. *arXiv preprint arXiv:1210.3335*, 2012.
- [10] Kenneth L. Clarkson and David P. Woodruff. Low rank approximation and regression in input sparsity time. *CoRR*, abs/1207.6365, 2012.
- [11] Paul G Constantine and David F Gleich. Tall and skinny qr factorizations in mapreduce architectures. In *Proceedings of the second international workshop on MapReduce and its applications*, pages 43–50. ACM, 2011.
- [12] Barbara Fadem. *High-yield behavioral science*. LWW, 2012.
- [13] Alex Gittens and Michael W Mahoney. Revisiting the nystrom method for improved large-scale machine learning. *arXiv preprint arXiv:1303.1849*, 2013.
- [14] Gene H. Golub and Charles F. Van Loan. *Matrix computations. 4th ed.* Baltimore, MD: The Johns Hopkins University Press, 4th ed. edition, 2013.
- [15] P. Gopalan, D. Mimno, S. Gerrish, M. Freedman, and D. Blei. Scalable inference of overlapping communities. In *Advances in Neural Information Processing Systems 25*, pages 2258–2266, 2012.
- [16] Joseph JáJá. *An introduction to parallel algorithms*. Addison Wesley Longman Publishing Co., Inc., 1992.
- [17] Brian Karrer and Mark EJ Newman. Stochastic blockmodels and community structure in networks. *Physical Review E*, 83(1):016107, 2011.
- [18] H.J. Kushner and G. Yin. *Stochastic Approximation and Recursive Algorithms and Applications*. Applications of Mathematics Series. Springer, 2003.
- [19] Andrea Lancichinetti and Santo Fortunato. Community detection algorithms: a comparative analysis. *Physical review E*, 80(5):056117, 2009.
- [20] Andrea Lancichinetti, Santo Fortunato, and János Kertész. Detecting the overlapping and hierarchical community structure in complex networks. *New Journal of Physics*, 11(3):033015, 2009.
- [21] F. McSherry. Spectral partitioning of random graphs. In *FOCS*, 2001.
- [22] J.L. Moreno. *Who shall survive?: A new approach to the problem of human interrelations*. Nervous and Mental Disease Publishing Co, 1934.

- [23] Tamás Nepusz, Andrea Petróczy, László Négyessy, and Fülöp Bazsó. Fuzzy communities and the concept of bridgeness in complex networks. *Physical Review E*, 77(1):016107, 2008.
- [24] Erkki Oja and Juha Karhunen. On stochastic approximation of the eigenvectors and eigenvalues of the expectation of a random matrix. *Journal of mathematical analysis and applications*, 106(1):69–84, 1985.
- [25] Pascal Pons and Matthieu Latapy. Computing communities in large networks using random walks. In *Computer and Information Sciences-ISCIS 2005*, pages 284–293. Springer, 2005.
- [26] Martin D Schatz, Tze Meng Low, Robert A van de Geijn, and Tamara G Kolda. Exploiting symmetry in tensors for high performance. *arXiv preprint arXiv:1301.7744*, 2013.
- [27] Robert R Sokal and F James Rohlf. The comparison of dendrograms by objective methods. *Taxon*, 11(2):33–40, 1962.
- [28] Jyothish Soman and Ankur Narang. Fast community detection algorithm with gpus and multicore architectures. In *Parallel & Distributed Processing Symposium (IPDPS), 2011 IEEE International*, pages 568–579. IEEE, 2011.
- [29] Korbinian Strimmer. fdrtool: a versatile r package for estimating local and tail area-based false discovery rates. *Bioinformatics*, 24(12):1461–1462, 2008.
- [30] Amanda L. Traud, Eric D. Kelsic, Peter J. Mucha, and Mason A. Porter. Comparing community structure to characteristics in online collegiate social networks. *SIAM Review*, in press (arXiv:0809.0960), 2010.
- [31] Jaewon Yang and Jure Leskovec. Defining and evaluating network communities based on ground-truth. In *Proceedings of the ACM SIGKDD Workshop on Mining Data Semantics*, page 3. ACM, 2012.
- [32] Yu Zhang and Dit-Yan Yeung. Overlapping community detection via bounded nonnegative matrix tri-factorization. In *Proceedings of the 18th ACM SIGKDD international conference on Knowledge discovery and data mining, KDD '12*, pages 606–614, New York, NY, USA, 2012. ACM.

7 Appendix

A Partitioning and Estimation of 3-stars

Consider a partition of nodes into sets X, A, B, C . A 3-star is a star graph with an internal node $x \in X$ and three leaves $\{a, b, c\}$ with $a \in A, b \in B, c \in C$. We refer to the internal node x of the star as its “head”, and denote the structure by $x \rightarrow \{a, b, c\}$ (see Figure 1). First, we count the number of 3-stars from X to A, B, C .

The tensor can be represented as

$$\mathbb{T}_{X \rightarrow \{A, B, C\}} := \frac{1}{|X|} \sum_{x \in X} [G_{x,A}^\top \otimes G_{x,B}^\top \otimes G_{x,C}^\top], \quad (5)$$

where \otimes denotes the *Kronecker product*, and $G_{x,A}$, $G_{x,B}$ and $G_{x,C}$ correspond to neighbourhood vectors drawn from the adjacency matrix G .

Theoretically, any random partition, where each set is of size $\Theta(n)$, has sufficient number of 3-stars to faithfully recover the mixed membership community model [2]. In practice, this holds for dense graphs, since there are sufficient number of 3-stars for any choice of partitioning. On the other hand, our real datasets consist of extremely sparse graphs, and we employ a simple heuristic to pick a good partition $\{X, A, B, C\}$ which yields sufficient number of 3-stars.

First, we arbitrarily pick disjoint sets X and $A \cup B \cup C$ of roughly the same size. We perform standard k -means algorithm to cluster nodes in $A \cup B \cup C$ into three groups \tilde{A} , \tilde{B} and \tilde{C} based on the Hamming distance between the vectors $\{G_{X \rightarrow i}^\top, i \in A \cup B \cup C\}$. We divide each set into three equal parts arbitrarily. We consider $\tilde{A} = \tilde{A}_1 \cup \tilde{A}_2 \cup \tilde{A}_3$, $\tilde{B} = \tilde{B}_1 \cup \tilde{B}_2 \cup \tilde{B}_3$ and $\tilde{C} = \tilde{C}_1 \cup \tilde{C}_2 \cup \tilde{C}_3$, and compute $A := \tilde{A}_1 \cup \tilde{B}_1 \cup \tilde{C}_1$. Similarly B and C are formed and we have the adjacency sub-matrices $G_{X,A}$, $G_{X,B}$ and $G_{X,C}$. This heuristic is fast since k -means with Hamming distance as a criterion is efficient.

B Dimensionality Reduction and Whitening

We derive the equations for whitening and STGD, and discuss our implementation details, including code design and optimization.

B.1 Whitening

Whitening step utilizes linear algebraic manipulations to make the tensor symmetric and orthogonal (in expectation). We note that a unique and tractable tensor decomposition is guaranteed for symmetric and orthogonal tensors [3]. A key insight in our implementation that contributes to significant speed-up of the overall algorithm and especially the whitening step is the computation of k -rank terms in the below equations. Then, the multiplications involve $O(n) \times (k)$ or $O(k) \times O(k)$ matrices and these are implemented the most efficient order of taking the sparse matrix products. Note that $k \ll n$. First we define $n_A = |A|$, $n_B = |B|$ and $n_C = |C|$.

1. *Symmetrization*: Using Theorem 3.6 from [3], we define pairs over Y_1 and Y_2 as $\text{Pairs}(Y_1, Y_2) := G_{X, Y_1}^\top \otimes G_{X, Y_2}^\top$. The transition matrices for B and C are computed as

$$Z_B := \text{Pairs}(A, C) (\text{Pairs}(B, C))^\dagger \quad (6)$$

$$Z_C := \text{Pairs}(A, B) (\text{Pairs}(C, B))^\dagger \quad (7)$$

Note that pseudoinverse of $(\text{Pairs}(B, C))$ can be computed using k-SVD :

$$\text{k-SVD}(\text{Pairs}(B, C)) = U_B(:, 1:k) \Sigma_{BC}(1:k) V_C(:, 1:k)^\top.$$

Although the whole term is in $n_B \times n_C$ space, we notice that the factors are in $n_B \times k$ and $n_C \times k$ space. This way, we propagate these products to next steps. This leads to a reduction in the required memory as well as the running time. The same applies for the pseudoinverse of $(\text{Pairs}(C, B))$. We then perform linear transformations for the partitions B and C to symmetrize the tensor of normalized 3-star counts.

We define

$$\tilde{G}_{X,B}^\top := Z_B G_{X,B}^\top \quad (8)$$

$$\tilde{G}_{X,C}^\top := Z_C G_{X,C}^\top \quad (9)$$

Now $G_{X,A}^\top$, $\tilde{G}_{X,B}^\top$ and $\tilde{G}_{X,C}^\top$ are of the same dimension, so that the tensor in Equation (5) is cubical, i.e., $\tilde{\text{T}}_{X \rightarrow \{A,B,C\}} \in \mathbb{R}^{n_A \times n_A \times n_A}$. Note that $\text{T}_{X \rightarrow \{A,B,C\}} \in \mathbb{R}^{n_A \times n_B \times n_C}$.

Until now, the implementation only involves matrix and vector multiplications and two SVDs.

2. *Orthogonalization*: Since our model assumes that community memberships are drawn from the Dirichlet distribution, we have to shift the moment terms according to Dirichlet moments so that the moments are centered. Recall that α_0 is the mixing parameter (Dirichlet concentration parameter), we shift M_2 to compute the centered $M_2^{\alpha_0}$:

We compute the shifted second moment matrix as

$$M_2^{\alpha_0} = \frac{1}{n_X} \sum_{x \in X} Z_C G_{x,C}^\top G_{x,B} Z_B^\top - \frac{\alpha_0}{\alpha_0 + 1} (\mu_{X \rightarrow A} \mu_{X \rightarrow A}^\top - \text{diag}(\mu_{X \rightarrow A} \mu_{X \rightarrow A}^\top)). \quad (10)$$

We first implement the k-SVD of $G_{X,C}^\top G_{X,B}$ since the $G_{X,C}^\top G_{X,B}$ to obtain a low rank approximation. Then the order in which the matrix products are carried out plays a significant role in terms of both memory and speed. We noticed that Z_C involves the multiplication of a sequence of matrices of sizes $\mathbb{R}^{n_A \times n_B}$, $\mathbb{R}^{n_B \times k}$, $\mathbb{R}^{k \times k}$, $\mathbb{R}^{k \times n_C}$, $G_{x,C}^\top G_{x,B}$ involving products of sizes $\mathbb{R}^{n_C \times k}$, $\mathbb{R}^{k \times k}$, $\mathbb{R}^{k \times n_B}$, and Z_B involving products of sizes $\mathbb{R}^{n_A \times n_C}$, $\mathbb{R}^{n_C \times k}$, $\mathbb{R}^{k \times k}$, $\mathbb{R}^{k \times n_B}$. While performing these products, we avoid products of sizes $\mathbb{R}^{O(n) \times O(n)}$ and $\mathbb{R}^{O(n) \times O(n)}$.

We compute the whitening matrix $W \in \mathbb{R}^{n_A \times k}$ such that $W^\top M_2^{\alpha_0} W = I$. The idea is that if the bilinear projection of the second order moment onto W results in the identity matrix, a trilinear projection of the third order moment onto W would result in the orthogonal tensor. We use multilinear operations to get an orthogonal and rank efficient tensor $\mathcal{T} = \text{T}_{X \rightarrow A, \bar{B}, \bar{C}}^{\alpha_0}(W, W, W)$.

Until now, we only implemented vector-vector products and one SVD.

The important aspect of our orthogonalization step is that we employ k-SVD instead of full SVD. The dimensionality reduction is crucial to the speed-up of the algorithm.

Overall, the whitening steps above involve 8 BLAS II, 19 BLAS III and 3 SVD operations.

B.2 Efficient code design using random projection and sparsity

When we consider very large-scale data, the whitening matrix is a bottleneck to handle when we aim for fast running times. We use two techniques in our implementation, namely:

1. Low rank approximation of matrices using the random projection method.
2. Sparse SVD computation via the Lanczos algorithm.

We give the overview of these methods below.

Randomized low rank approximation: From [13], for the low k -rank positive semi-definite matrix $M_2^{\alpha_0} \in \mathbb{R}^{n_A \times n_A}$ with $n_A \gg k$, we can perform random projection to reduce dimensionality. More precisely, if we have a random matrix $S \in \mathbb{R}^{n_A \times \bar{k}}$ with unit norm (rotation matrix), we project $M_2^{\alpha_0}$ onto this random matrix to get $\mathcal{C} := M_2^{\alpha_0} S \in \mathbb{R}^{n_A \times \bar{k}}$. Note that we choose $\bar{k} = 2k$ in our implementation. The range of \mathcal{C} is thus the same as the range of $M_2^{\alpha_0}$. If we define $D := S^\top M_2^{\alpha_0} S \in \mathbb{R}^{\bar{k} \times \bar{k}}$, then a low rank approximation of $M_2^{\alpha_0}$ is $\mathcal{C} D^\dagger \mathcal{C}^\top$ [13].

Recall that the definition of a whitening matrix W is that $W^\top M_2^{\alpha_0} W = I$. We can obtain the whitening matrix of $M_2^{\alpha_0}$ without directly doing a SVD on $M_2^{\alpha_0} \in \mathbb{R}^{n_A \times n_A}$ in two different ways namely, using tall-thin SVD and tall-thin QR.

1. *Tall-thin SVD:* The whitening matrix can be obtained by

$$W = (\mathcal{C}^\dagger)^\top (D^{\frac{1}{2}})^\top. \quad (11)$$

Therefore, we only need to compute SVD of a tall-thin matrix $\mathcal{C} \in \mathbb{R}^{n_A \times \bar{k}}$. Note that $D \in \mathbb{R}^{\bar{k} \times \bar{k}}$, its square-root is easy to compute. Similarly, pseudoinverses can also be obtained without directly doing SVD. For instance, the pseudoinverse of the Pairs(B, C) matrix is given by

$$(\text{Pairs}(B, C))^\dagger = (\Xi^\dagger)^\top \Psi \Xi^\dagger,$$

where $\Psi = S^\top (\text{Pairs}(B, C)) S$ and $\Xi = (\text{Pairs}(B, C)) S$.

2. *Tall-thin QR*: In this method, we compute the whitening matrix also as in Eq (11). The difference is that we instead implement a tall-thin QR on \mathcal{C} , therefore the whitening matrix is obtained as

$$W = Q(R^\dagger)^\top (D^{\frac{1}{2}})^\top.$$

Sparsity: We also take advantage of the sparse representation [10] to resolve memory issues that arise when running large scale datasets such as the DBLP dataset. We implement our algorithm using the sparse matrix format and operations available in the Eigen toolkit⁵ and we use the SVDLIBC [8] library to compute sparse SVD via the Lanczos algorithm. This allows for scalability on a single machine to a dataset having about a million nodes.

C Stochastic Updates

After obtaining the whitening matrix, we whiten the data $G_{x,A}^\top$, $G_{x,B}^\top$ and $G_{x,C}^\top$ by linear operations to get g_A^t , g_B^t and $g_C^t \in \mathbb{R}^k$:

$$\begin{aligned} g_A^t &:= \langle G_{x,A}^\top, W \rangle, \\ g_B^t &:= \langle Z_B G_{x,B}^\top, W \rangle, \\ g_C^t &:= \langle Z_C G_{x,C}^\top, W \rangle. \end{aligned}$$

where $x \in X$ and t denotes the index of the online data.

The stochastic gradient descent algorithm is obtained by taking the derivative of the loss function $\frac{\partial L^t(\mathbf{v})}{\partial v_i}$:

$$\frac{\partial L^t(\mathbf{v})}{\partial v_i} = 3\theta \sum_{j=1}^k \langle v_j, v_i \rangle^2 v_j - \langle v_i, g_A^t \rangle \langle v_i, g_B^t \rangle g_C^t - \langle v_i, g_B^t \rangle \langle v_i, g_C^t \rangle g_A^t - \langle v_i, g_A^t \rangle \langle v_i, g_C^t \rangle g_B^t$$

for $i \in [k]$, where g_A^t , g_B^t and g_C^t are the online whitened data points as discussed in the whitening step and θ is a constant factor that we can set.

The iterative updating equation for the stochastic gradient update is given by

$$\phi_i^{t+1} \leftarrow \phi_i^t - \beta^t \frac{\partial L^t}{\partial v_i} \Big|_{\phi_i^t} \quad (12)$$

for $i \in [k]$, where β^t is the learning rate, ϕ_i^t is the last iteration eigenvector and ϕ_i^t is the updated eigenvector. We update eigenvectors through

$$\phi_i^{t+1} \leftarrow \phi_i^t - 3\theta\beta^t \sum_{j=1}^k \left[\langle \phi_j^t, \phi_i^t \rangle^2 \phi_j^t \right] \quad (13)$$

$$+ 3\beta^t \langle \phi_i^t, g_A^t \rangle \langle \phi_i^t, g_B^t \rangle g_C^t \quad (14)$$

Now we shift the updating steps so that they are centered: term (14) is

$$3\beta^t \langle \phi_i^t, g_A^t \rangle \langle \phi_i^t, g_B^t \rangle g_C^t \quad (15)$$

$$:= 3\beta^t \langle \phi_i^t, g_A^t \rangle \langle \phi_i^t, g_B^t \rangle g_C^t \quad (16)$$

$$+ 3\beta^t \frac{2\alpha_0^2}{(\alpha_0 + 1)(\alpha_0 + 2)} \langle \phi_i^t, \mu_A \rangle \langle \phi_i^t, \mu_B \rangle \mu_C \quad (17)$$

$$+ 3\beta^t \frac{\alpha_0}{\alpha_0 + 2} \langle \phi_i^t, g_A^t \rangle \langle \phi_i^t, g_B^t \rangle \mu_C \quad (18)$$

$$+ 3\beta^t \frac{\alpha_0}{\alpha_0 + 2} \langle \phi_i^t, g_A^t \rangle \langle \phi_i^t, \mu_B \rangle g_C \quad (19)$$

$$+ 3\beta^t \frac{\alpha_0}{\alpha_0 + 2} \langle \phi_i^t, \mu_A \rangle \langle \phi_i^t, g_B^t \rangle g_C, \quad (20)$$

⁵http://eigen.tuxfamily.org/index.php?title=Main_Page

where $\mu_A := \mathbb{E}_t[g_A^t]$ and similarly for μ_B and μ_C .

C.1 Optimization of STGD

After whitening, the STGD requires the most code design and optimization effort, and so we convert that into BLAS-like routines.

Efficient STGD via stacked vector operations: Although the updating equation for the stochastic gradient update is presented serially, we can update the k eigenvectors simultaneously in parallel. The basic idea is to stack the k eigenvectors $\phi_i \in \mathbb{R}^k$ into a matrix Φ , then using the internal parallelism designed for BLAS III operations. Since the eigenvectors are just k length k vectors, we store them in the device memory and perform the iterations.

Note that we have many common terms in (16), (19) and (20) when updating the coefficient of g_C^t and many common terms as well in (17), (18) when updating the coefficient of μ_C^t , we use the duplications to stack those inner product terms into matrix and employ BLAS III products as follows. We stack the vectors $g_A^t, g_B^t, \mu_A, \mu_B$ to form a $4 \times k$ matrix \mathcal{S} . We call this *iteration matrix*. Compute the product with the current eigenvector matrix $\mathcal{S} \Phi$ to get two $4 \times k$ matrices of scalars which are used to scale the g_C and μ_C terms.

1. We scale g_C by $(\alpha_0 + 1)(\alpha_0 + 2)g_A g_B - \alpha_0(\alpha_0 + 1)g_A \mu_B - \alpha_0(\alpha_0 + 1)\mu_A g_B$. Define the vector $u = [\mu_A \ \mu_B \ g_A \ g_B]^\top$. So we want a scaling matrix \mathcal{J}_1 to compute the quadratic form: $u^\top \mathcal{J}_1 u = (\alpha_0 + 1)(\alpha_0 + 2)g_A g_B - \alpha_0(\alpha_0 + 1)g_A \mu_B - \alpha_0(\alpha_0 + 1)\mu_A g_B$. Solving for this, we obtain

$$\mathcal{J}_1 = \begin{pmatrix} 0 & 0 & 0 & 0 \\ 0 & 0 & \frac{-\alpha_0}{\alpha_0+2} & 0 \\ 0 & 0 & 0 & 0 \\ \frac{-\alpha_0}{\alpha_0+2} & 0 & 1 & 0 \end{pmatrix} \quad (21)$$

2. Similar to the scaling matrix \mathcal{J}_1 , we compute the scaling matrix for μ_C . Now we solve for B such that $u^\top \mathcal{J}_2 u = 2\alpha_0^2 \mu_A \mu_B - \alpha_0(\alpha_0 + 1)g_A g_B$. We obtain:

$$\mathcal{J}_2 = \begin{pmatrix} 0 & 0 & 0 & 0 \\ \frac{2\alpha_0^2}{(\alpha_0+1)(\alpha_0+2)} & 0 & 0 & 0 \\ 0 & 0 & 0 & 0 \\ 0 & 0 & \frac{-\alpha_0}{\alpha_0+2} & 0 \end{pmatrix} \quad (22)$$

Next we form the vector of scalars $[u_1^\top \mathcal{J}_1 u_1 \dots u_k^\top \mathcal{J}_1 u_k]$ corresponding to the k eigenvectors, and similarly $[u_1^\top \mathcal{J}_2 u_1 \dots u_k^\top \mathcal{J}_2 u_k]$. Note that these are $\text{diag}[U^\top \mathcal{J}_1 U]$ and $\text{diag}[U^\top \mathcal{J}_2 U]$ and \mathcal{J}_1 and \mathcal{J}_2 are sparse.

Overall, the STGD step involves $1 + k + i(2 + 3k)$ BLAS II over \mathbb{R}^k vectors, $7N$ BLAS III over $\mathbb{R}^{k \times k}$ matrices and 2 QR operations over $\mathbb{R}^{k \times k}$ matrices, where i denotes the number of iterations.

C.2 Post processing

Eigenvalues $\Lambda := [\lambda_1, \lambda_2, \dots, \lambda_k]$ are estimated as the norm of the eigenvectors $\lambda_i = \|\phi_i\|^3$. After we obtain Λ and Φ , we compute the community membership matrix via $\hat{\Pi}_{A^c} = \text{Thres} \left(\gamma \text{diag}(\Lambda)^{-1} \Phi^\top \hat{W}^\top G_{A^c, A}^\top, \tau \right)$, where $\text{Thres}(\cdot, \tau)$ denotes thresholding with parameter τ , i.e. setting entries less than τ to zero. Similarly, we estimate $\hat{\Pi}_A$. Next, we have, $\hat{\alpha}_i = \gamma^2 \lambda_i^{-2}, \forall i \in [k]$, where γ^2 is chosen such that we have normalization $\sum_{i \in [k]} \hat{\alpha}_i := \sum_{i \in [k]} \frac{\alpha_i}{\alpha_0} = 1$.

Thus, we perform STGD method to estimate the eigenvectors and eigenvalues of the whitened tensor, and then use these to estimate the community membership matrix $\hat{\Pi}$ by thresholding.

D Proof of correctness of our algorithm:

We presented our algorithm implementation details in Appendices A, B and C. We now prove the correctness of our algorithm.

First, we compute M_2 as just

$$\mathbb{E}_x \left[\tilde{G}_{x,C}^\top \otimes \tilde{G}_{x,B}^\top \mid \Pi_A, \Pi_B, \Pi_C \right]$$

Since we define

$$\begin{aligned} \tilde{G}_{x,B}^\top &:= \mathbb{E}_x \left[G_{x,A}^\top \otimes G_{x,C}^\top \mid \Pi_A, \Pi_C \right] \left(\mathbb{E}_x \left[G_{x,B}^\top \otimes G_{x,C}^\top \mid \Pi_B, \Pi_C \right] \right)^\dagger G_{x,B}^\top \\ \tilde{G}_{x,C}^\top &:= \mathbb{E}_x \left[G_{x,A}^\top \otimes G_{x,B}^\top \mid \Pi_A, \Pi_B \right] \left(\mathbb{E}_x \left[G_{x,C}^\top \otimes G_{x,B}^\top \mid \Pi_B, \Pi_C \right] \right)^\dagger G_{x,C}^\top. \end{aligned}$$

We obtain that $M_2 = F_A (\mathbb{E}_x [\pi_x \pi_x^\top]) F_A^\top$, where F_A is defined as $F_A := \Pi^\top P^\top$. Note that P is the community connectivity matrix defined as $P \in [0, 1]^{k \times k}$. Now that we know M_2 , $\mathbb{E} [\pi_i^2] = \frac{\alpha_i(\alpha_i+1)}{\alpha_0(\alpha_0+1)}$, and $\mathbb{E} [\pi_i \pi_j] = \frac{\alpha_i \alpha_j}{\alpha_0(\alpha_0+1)} \forall i \neq j$, we can get the centered second order moments $M_2^{\alpha_0}$ as

$$M_2^{\alpha_0} := F_A \text{diag} \left(\left[\frac{\alpha_1 \alpha_1 + 1}{\alpha_0(\alpha_0 + 1)}, \dots, \frac{\alpha_k \alpha_k + 1}{\alpha_0(\alpha_0 + 1)} \right] \right) F_A^\top \quad (23)$$

$$= M_2 - \frac{\alpha_0}{\alpha_0 + 1} F_A (\hat{\alpha} \hat{\alpha}^\top - \text{diag}(\hat{\alpha} \hat{\alpha}^\top)) F_A^\top \quad (24)$$

$$= \frac{1}{n_X} \sum_{x \in X} Z_C G_{x,C}^\top G_{x,B} Z_B^\top - \frac{\alpha_0}{\alpha_0 + 1} (\mu_{X \rightarrow A} \mu_{X \rightarrow A}^\top - \text{diag}(\mu_{X \rightarrow A} \mu_{X \rightarrow A}^\top)) \quad (25)$$

Thus, our whitening matrix is computed. Now, our whitened tensor is \mathcal{T} is given by

$$\mathcal{T} = \mathbb{T}_{X \rightarrow A, \tilde{B}, \tilde{C}}^{\alpha_0}(W, W, W) = \frac{1}{n_X} \sum_x [(W^\top F_A \pi_x^{\alpha_0}) \otimes (W^\top F_A \pi_x^{\alpha_0}) \otimes (W^\top F_A \pi_x^{\alpha_0})],$$

where $\pi_x^{\alpha_0}$ is the centered vector so that $\mathbb{E}[\pi_x^{\alpha_0} \otimes \pi_x^{\alpha_0} \otimes \pi_x^{\alpha_0}]$ is diagonal. We then apply the stochastic gradient descent technique to decompose the third order moment.

E GPU Architecture

The algorithm we propose is very amenable to parallelization and is scalable which makes it suitable to implement on processors with multiple cores in it. Our method consists of simple linear algebraic operations, thus enabling us to utilize *Basic Linear Algebra Subprograms* (BLAS) routines such as BLAS I (vector operations), BLAS II (matrix-vector operations), BLAS III (matrix-matrix operations), Singular Value Decomposition (SVD), and iterative operations such as stochastic gradient descent for tensor decomposition that can easily take advantage of Single Instruction Multiple Data (SIMD) hardware units present in the GPUs. As such, our method is amenable to parallelization and is ideal for GPU-based implementation.

Overview of code design: From a higher level point of view, a typical GPU based computation is a three step process involving data transfer from CPU memory to GPU global memory, operations on the data now present in GPU memory and finally, the result transfer from the GPU memory back to the CPU memory. We use the CULA library for implementing the linear algebraic operations.

GPU compute architecture: The GPUs achieve massive parallelism by having hundreds of homogeneous processing cores integrated on-chip. Massive replication of these cores provides the parallelism needed by the applications that run on the GPUs. These cores, for the Nvidia GPUs, are known as *CUDA cores*, where each core has fully pipelined floating-point and integer arithmetic logic units. In Nvidia’s Kepler architecture based GPUs, these CUDA cores are bunched together to form a *Streaming Multiprocessor* (SMX). These SMX units act as the basic building block for Nvidia Kepler GPUs. Each GPU contains multiple SMX units where each SMX unit has 192 single-precision CUDA cores, 64 double-precision units, 32 special function units, and 32 load/store units for data movement between cores and memory.

Each SMX has L1, shared memory and a read-only data cache that are common to all the CUDA cores in that SMX unit. Moreover, the programmer can choose between different configurations of the shared memory and L1 cache. Kepler GPUs also have an L2 cache memory of about 1.5MB that is common to all the on-chip SMXs. Apart from the above mentioned memories, Kepler based GPU cards come with a large DRAM memory, also known as the global memory, whose size is usually in gigabytes. This global memory is also visible to all the cores. The GPU cards usually do not exist as standalone devices. Rather they are part of a CPU based system, where the CPU and GPU interact with each other via PCI (or PCI Express) bus.

In order to program these massively parallel GPUs, Nvidia provides a framework known as *CUDA* that enables the developers to write programs in languages like C, C++, and Fortran etc. A CUDA program constitutes of functions called *CUDA kernels* that execute across many parallel software threads, where each thread runs on a CUDA core. Thus the GPU’s performance and scalability is exploited by the simple partitioning of the algorithm into fixed sized blocks of parallel threads that run on hundreds of CUDA cores. The threads running on an SMX can synchronize and cooperate with each other via the shared memory of that SMX unit and can access the Global memory. Note that the CUDA kernels are launched by the CPU but they get executed on the GPU. Thus compute architecture of the GPU requires CPU to initiate the CUDA kernels.

CUDA enables the programming of Nvidia GPUs by exposing low level API. Apart from CUDA framework, Nvidia provides a wide variety of other tools and also supports third party libraries that can be used to program Nvidia GPUs. Since a major chunk of the scientific computing algorithms is linear algebra based, it is not surprising that the standard linear algebraic solver libraries like BLAS and *Linear Algebra PACKage* (LAPACK) also have their equivalents for Nvidia GPUs in one form or another. Unlike CUDA APIs, such libraries expose APIs at a much higher-level and mask the architectural details of the underlying GPU hardware to some extent thus enabling relatively faster development time.

Considering the tradeoffs between the algorithm’s computational requirements, design flexibility, execution speed and development time, we choose *CULA-Dense* as our main implementation library. CULA-Dense provides GPU based implementations of the LAPACK and BLAS libraries for dense linear algebra and contains routines for systems solvers, singular value decompositions, and eigen-problems. Along with the rich set of functions that it offers, CULA provides the flexibility needed by the programmer to rapidly implement the algorithm while maintaining the performance. It hides most of the GPU architecture dependent programming details thus making it possible for rapid prototyping of GPU intensive routines.

The data transfers between the CPU memory and the GPU memory are usually explicitly initiated by CPU and are carried out via the PCI (or PCI Express) bus interconnecting the CPU and the GPU. The movement of data buffers between CPU and GPU is the most taxing in terms of time. The buffer transaction time is shown in the plot in Figure 6. Newer GPUs, like Kepler based GPUs, also support useful features like GPU-GPU direct data transfers without CPU intervention. Our system and software specifications are given in Table 7.

Hardware / software	Version
CPU	Dual 8-core Xeon @ 2.0GHz
Memory	64GB DDR3
GPU	Nvidia Quadro K5000
CUDA Cores	1536
Global memory	4GB GDDR5
CentOS	Release 6.4 (Final)
GCC	4.4.7
CUDA	Release 5.0
CULA-Dense	R16a

Table 7: System specifications.

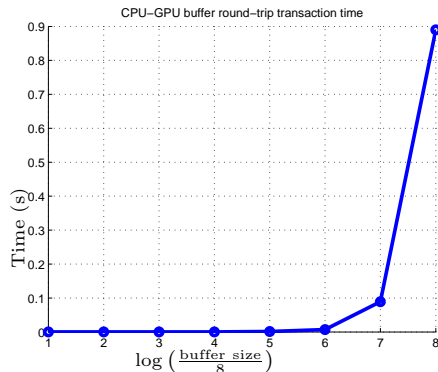


Figure 6: Experimentally measured time taken for buffer transfer between the CPU and the GPU memory in our system.

CULA exposes two important interfaces for GPU programming namely, *standard* and *device*. Using the standard interface, the developer can program without worrying about the underlying architectural details of the GPU as the standard interface takes care of all the data movements, memory allocations in the GPU and synchronization issues. This however comes at a cost. For every standard interface function call the data is moved in and out of the GPU even if the output result of one operation is directly required by the subsequent operation. This unnecessary movement of intermediate data can dramatically impact the performance of the program. In order to avoid this, CULA provides the device interface. We use the device interface for STGD in which the programmer is responsible for data buffer allocations in the GPU memory, the required data movements between the CPU and GPU, and operates only on the data in the GPU. Thus the subroutines of the program that are iterative in nature are good candidates for device implementation.

Pre-processing and post-processing: The pre-processing involves matrices whose leading dimension is of the order of number of nodes. These are implemented using the CULA standard interface BLAS II and BLAS III routines.

Pre-processing requires SVD computations for the Moore-Penrose pseudoinverse calculations. We use CULA SVD routines since these SVD operations are carried out on matrices of moderate size. We further replaced the CULA SVD routines with more scalable SVD and pseudo inverse routines using random projections [13] to handle larger datasets such as DBLP dataset in our experiment.

After STGD, the community membership matrix estimates are obtained using BLAS III routines provided by the CULA standard interface. The matrices are then used for hypothesis testing to evaluate the algorithm against the ground truth.

F Additional Results on Datasets

F.1 Results on Synthetic Datasets

We perform experiments for both the stochastic block model ($\alpha_0 = 0$) and the mixed membership model. For the mixed membership model, we set the concentration parameter $\alpha_0 = 1$. We note that the error is around 8% – 14% and the running times are under a minute, when $n \leq 10000$ and $n \gg k$.

We observe that more samples result in a more accurate recovery of memberships which matches intuition and theory. Overall, our learning algorithm performs better in the stochastic block model case than in the mixed membership model case although we note that the accuracy is quite high for practical purposes. Theoretically, this is expected since smaller concentration parameter α_0 is easier for our algorithm to learn [2]. Also, our algorithm is scalable to an order of magnitude more in n as illustrated by experiments on real-world large-scale datasets.

Note that we threshold the estimated memberships to clean the results. There is a tradeoff between match ratio and average error via different thresholds. In synthetic experiments, the tradeoff is not evident since a perfect matching is always present. However, we need to carefully handle this in experiments involving real data.

F.2 Further results on the Facebook dataset

A snapshot of the Facebook network of UNC [30] is provided with user attributes. The ground truth communities are based on user attributes given in the dataset which are not exposed to the algorithm. There are 360 top communities with sufficient (at least 20) users. Our algorithm can recover these attributes with high accuracy; see main paper for our method’s results compared with variational inference result [15].

We also obtain results for a range of values of α_0 (Figure 7). We observe that the recovery ratio improves with larger α_0 since a larger α_0 can recover overlapping communities more efficiently while the error score remains relatively the same.

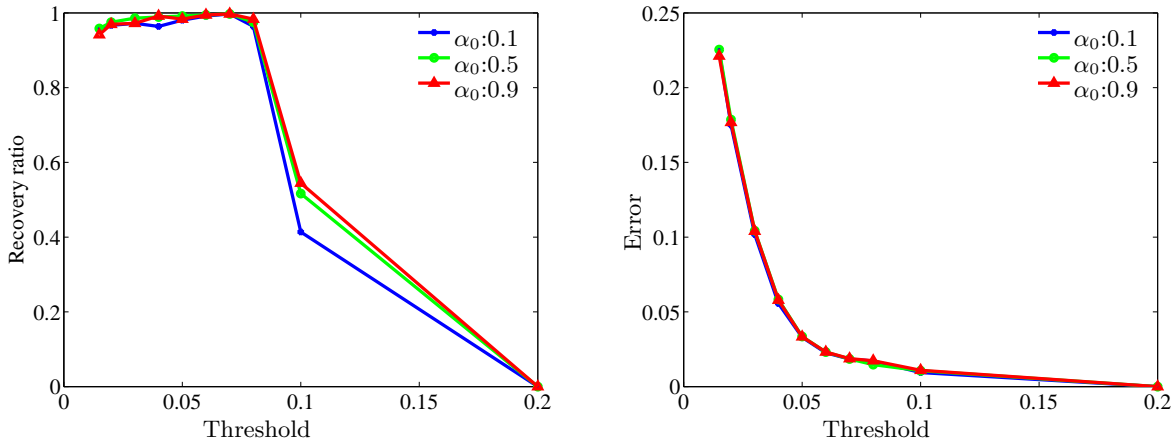


Figure 7: Performance analysis of Facebook dataset under different settings of the concentration parameter (α_0) for $\hat{k} = 100$.

F.3 Clean-up of the Yelp dataset

Among all 11537 businesses, there are 89.39% of them are still open. We only select those businesses which are still open. There are 285 categories in total. After we remove all the categories having no more than 20 businesses within it, there are 134 categories that remain. We generate community membership matrix

for business categories $\Pi_c \in \mathbb{R}^{k_c \times n}$ where $k_c := 134$ is the number of remaining categories and $n := 10141$ is the number of business remaining after removing all the negligible categories. All the businesses collected in the Yelp data are in AZ except 3 of them (one is in CA, one in CO and the other in SC). We remove the three businesses outside AZ. We notice that most of the businesses are spread out in 25 cities. Community membership matrix for location is defined as $\Pi \in \mathbb{R}^{k_l \times n}$ where $k_l := 25$ is the number cities and $n := 10010$ is number of businesses. Distribution of locations are in Table 9. The stars a business receives can vary from 1 (the lowest) to 5 (the highest). The higher the score is, the more satisfied the customers are. The average star score is 3.6745. The distribution is given in Table 8. There are also review counts for each business which are the number of reviews that business receives from all the users. The minimum review counts is 3 and the maximum is 862. The mean of review counts is 20.1929. The preprocessing helps us to pick out top communities.

There are 5 attributes associated with all the 11537 businesses, which are “open”, “Categories”, “Location”, “Review Counts” and “Stars”. We model ground truth communities as a combination of “Categories” and “Location”. We select business categories with more than 20 members and remove all businesses which are closed. 10010 businesses are remained. Only 28588 users are involved in reviews towards the 10010 businesses. There are 3 attributes associated with all the 28588 users, which are “Female”, “Male”, “Review Counts” and “Stars”. Although we do not directly know the gender information from the dataset, a name-gender guesser⁶ is used to estimate gender information using names.

Star Score	Num of businesses	Percentage
1.0	108	0.94%
1.5	170	1.47%
2.0	403	3.49%
2.5	1011	8.76%
3.0	1511	13.10%
3.5	2639	22.87%
4.0	2674	23.18%
4.5	1748	15.15%
5.0	1273	11.03%

Table 8: Table for distribution of business star scores.

F.4 Further results on the Yelp dataset

We provide some sample visualization results in Figure 8 for both the ground truth and the estimates from our algorithm. We sub-sample the users and businesses, group the users into male and female categories, and consider nail salon and tire businesses. Analysis of ground truth reveals that nail salon and tire businesses are very discriminative of the user genders, and thus we employ them for visualization. We note that both the nail salon and tire businesses are categorized with high accuracy, while users are categorized with poorer accuracy.

Our algorithm can also recover the attributes of users. However, the ground truth available about users is far more limited than businesses, and we only have information on gender, average review counts and average stars (we infer the gender of the users through their names). Our algorithm can recover all these attributes. We observe that gender is the hardest to recover while review counts is the easiest. We see that the other user attributes recovered by our algorithm correspond to valuable user information such as their interests, location, age, lifestyle, etc. This is useful, for instance, for businesses studying the characteristics of their users, for delivering better personalized advertisements for users, and so on.

⁶ <https://github.com/amacinho/Name-Gender-Guesser> by Amac Herdagdelen.

City	State	Num of business
Anthem	AZ	34
Apache Junction	AZ	46
Avondale	AZ	129
Buckeye	AZ	31
Casa Grande	AZ	48
Cave Creek	AZ	65
Chandler	AZ	865
El Mirage	AZ	11
Fountain Hills	AZ	49
Gilbert	AZ	439
Glendale	AZ	611
Goodyear	AZ	126
Laveen	AZ	22
Maricopa	AZ	31
Mesa	AZ	898
Paradise Valley	AZ	57
Peoria	AZ	267
Phoenix	AZ	4155
Queen Creek	AZ	78
Scottsdale	AZ	2026
Sun City	AZ	37
Surprise	AZ	161
Tempe	AZ	1153
Tolleson	AZ	22
Wickenburg	AZ	28

Table 9: Distribution of business locations. Only top cities with more than 10 businesses are presented.

F.5 Further results on the DBLP dataset

The DBLP data contains bibliographic records⁷ with various publication venues, such as journals and conferences, which we model as communities. We then consider authors who have published at least one paper in a community (publication venue) as a member of it. Co-authorship is thus modeled as link in the graph in which authors are represented as nodes. We generate a subsample of 116,317 authors who are highly active within the last 7 years in top 250 communities (with most active authors). We also run on the whole dataset with 1,054,066 authors in 6003 communities.

We select top 10 communities which are recovered with the lowest error and report the author with the highest weight in $\hat{\Pi}$ for those top 10 communities. Among the matched communities, we find the author with the highest membership weight illustrated in Table 10. Note that this is different from author reputation which we do not analyze due to lack of citation data for each paper in DBLP dataset. Conceivably, when such citation data is available, our method can recover impactful authors across different communities.

Venue	Authors				
GECCO	Edward H. Shortliffe	Anne Siegel	Jiangtao Wen	Fei Xiong	Dragoljub Pokrajac
CISIS	Lili Liu	Salah-Eddine Tbahriti	Michael J. Lee	Taishi Takasawa	Behrouz Touri
IEEE SCC	Nilima Nigam	Vladimir Despotovic	Cdric Baradat	Muhammad Sabir Idrees	Toshihiro Matsui
ACL	Atulya K. Nagar	Raluca Gera	Yoshiyasu Okuhara	Mohamed Abid	Tim Leung
I J Bif & Ch	Dongsheng Zhao	Christian P. Robert	Dong-Sung Ryu	David Klatzmann	Noriko Matsumoto
ICCSA	Bundit Laekhanukit	Deepak Bal	Robson Costa	Zhaohui Peng	Antonio M. Rodriguez-Chia
CMPB	Po-Chou Chan	Yanyan Du	Akihiro Minagawa	Peter J. Stuekey	Xingyu Ma
I J Comp Math	Norbert Elkmann	Waixi Liu	Amitava Datta	Barbara Paech	Christine Legner
JMLR	Lim Choo Min	Mirosław Malek	Sally Safwat	Tianshuang Qiu	Monson H. Hayes
OTM w.shops	Ning Qiu	Vojkan Davidovic	Antonis Bikakis	Marina Groshaus	Silvija Kokalj-Filipovic

Table 10: Top recovered publication venues with lowest error and authors with highest membership weights in $\hat{\Pi}$ for DBLP dataset.

Bridgeness in overlapping communities is an interesting measure to evaluate in the network. Bridge is defined as a vertex that crosses structural holes between discrete groups of people, while bridgeness analyzes to what extent a given vertex is shared among different communities [23]. We again display the top bridging nodes recovered by our method for DBLP dataset in Table 11.

⁷<http://dblp.uni-trier.de/xml/Dblp.xml>

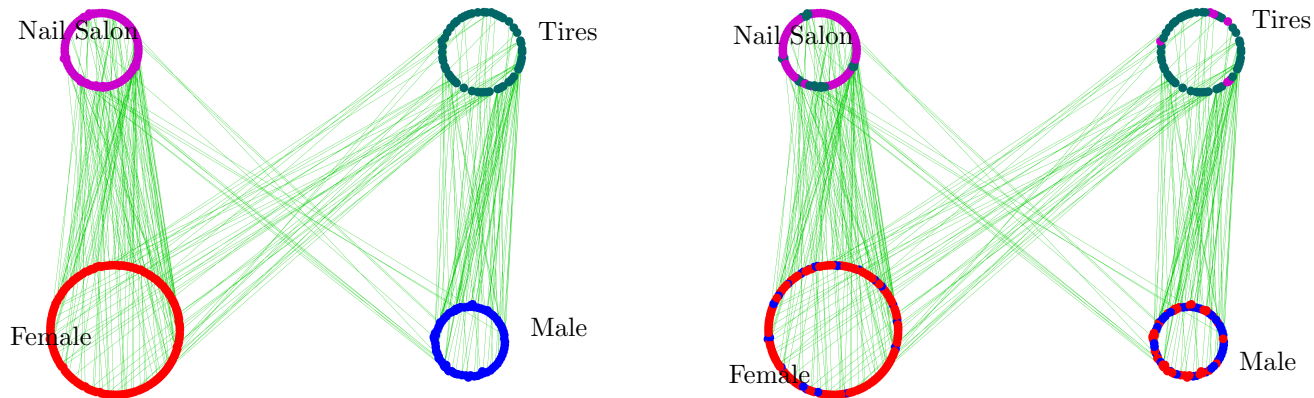


Figure 8: Ground truth (left) vs estimated business and user categories (right). The error in the estimated graph due to misclassification is shown by the mixed colours.

top 1~5	top 6~10	top 11~15	top 16~20	top 21~25
Wen Gao	Yan Zhang	Jiawei Han	Atsuo Takanishi	Yang Yang
Paul M. Thompson	Wei Wang	Xuemin Shen	Yu Zhang	Ming Li
Piet Demeester	Francky Catthoor	Jing Li	Rik Van de Walle	Nassir Navab
Yang Liu	Arthur W. Toga	Xin Li	Hiroshi G. Okuno	Lei Wang
Wei Liu	Thomas S. Huang	Lajos Hanzo	Hiroshi Harada	Li Zhang

Table 11: Top 25 bridging authors in DBLP.